THE ASTROPHYSICAL JOURNAL, 912:30 (14pp), 2021 May 1 https://doi.org/10.3847/1538-4357/abe765

Calcium-rich Transient SN 2019ehk in a Star-forming Environment: Yet Another Candidate for a Precursor of a Double Neutron-star Binary

Tatsuya Nakaoka[1,2], Keiichi Maeda[3], Masayuki Yamanaka[4], Masaomi Tanaka[5], Miho Kawabata[4], Takashi J. Moriya[6,7], Koji S. Kawabata[1,2], Nozomu Tominaga[8,9], Kengo Takagi[2], Fumiya Imazato[2], Tomoki Morokuma[10], Shigeyuki Sako[10], Ryou Ohsawa[10], Takashi Nagao[11], Ji-an Jiang[9], Umut Burgaz[3,12], Kenta Taguchi[3], Makoto Uemura[1,2], Hiroshi Akitaya[1,2,13], Mahito Sasada[1,2], Keisuke Isogai[4,14], Masaaki Otsuka[4], and Hiroyuki Maehara[15]

[1] Hiroshima Astrophysical Science Center, Hiroshima University, Kagamiyama 1-3-1, Higashi-Hiroshima , Hiroshima 739-8526, Japan;nakaokat@hiroshima-u.ac.jp
[2] Department of Physical Science, Hiroshima University, Kagamiyama 1-3-1, Higashi-Hiroshima 739-8526, Japan
[3] Department of Astronomy, Kyoto University, Kitashirakawa-Oiwake-cho, Sakyo-ku, Kyoto 606-8502, Japan
[4] Okayama Observatory, Kyoto University, 3037-5 Honjo, Kamogatacho, Asakuchi, Okayama 719-0232, Japan
[5] Astronomical Institute, Graduate School of Science, Tohoku University, Aramaki, Aoba, Sendai 980-8578, Japan
[6] National Astronomical Observatory of Japan, 2-21-1 Osawa, Mitaka, Tokyo 181-8588, Japan
[7] School of Physics and Astronomy, Faculty of Science, Monash University, Clayton, Victoria 3800, Australia
[8] Department of Physics, Faculty of Science and Engineering, Konan University, Kobe, Hyogo 658-8501, Japan
[9] Kavli Institute for the Physics and Mathematics of the Universe (WPI), The University of Tokyo Institutes for Advanced Study, The University of Tokyo, 5-1-5 Kashiwanoha, Kashiwa, Chiba 277-8583, Japan
[10] Institute of Astronomy, Graduate School of Science, The University of Tokyo, 2-21-1 Osawa, Mitaka, Tokyo 181-0015, Japan
[11] European Southern Observatory, Karl-Schwarzschild-Str 2, D-85748 Garching b. München, Germany
[12] Department of Astronomy and Space Sciences, Ege University, 35100, İzmir, Turkey
[13] Planetary Exploration Research Center, Chiba Institute of Technology, 2-17-1 Tsudanuma, Narashino, Chiba 275-0016, Japan
[14] Department of Multi-Disciplinary Sciences, Graduate School of Arts and Sciences, The University of Tokyo, 3-8-1 Komaba, Meguro, Tokyo 153-8902, Japan
[15] Subaru Telescope Okayama Branch Office, National Astronomical Observatory of Japan, National Institutes of Natural Sciences, 3037-5 Honjo, Kamogata, Asakuchi, Okayama 719-0232, Japan

Received 2020 March 27; revised 2021 February 2; accepted 2021 February 3; published 2021 April 30

Abstract

We present optical and near-infrared observations of SN 2019ehk, which was initially reported as a Type Ib supernova (SN). We show that it evolved to a Ca-rich transient according to its spectral properties and evolution in late phases. However, it shows a few properties distinct from those of the canonical Ca-rich transients: a short-duration first peak in the light curve, high peak luminosity, and association with a star-forming environment. Indeed, some of these features are shared with iPTF14gqr and iPTF16hgs, which are candidates for a special class of core-collapse SNe: the so-called ultra-stripped envelope SNe, i.e., a relatively low-mass He (or C+O) star explosion in a binary as a precursor of short-period double neutron star (NS) binaries. The estimated ejecta mass ($0.4M_{\odot}$) and explosion energy (1.7×10^{50} erg) are consistent with this scenario. The analysis of the first peak suggests the existence of dense circumstellar material in the vicinity of the progenitor, implying a CCSN origin. Based on this analysis, we suggest SN 2019ehk is another candidate for a low-mass He star explosion. It might create a double NS binary, but with a wide separation. These candidates for low-mass stripped envelope SNe, including ultra-stripped envelope SN candidates, seem to form a subpopulation among Ca-rich transients, associated with young population. We propose that the key to distinguishing this population is the early first peak in their light curves.

Unified Astronomy Thesaurus concepts: Supernovae (1668)

1. Introduction

Over the last decade, some peculiar transients that show characteristics different from those of canonical supernovae (SNe) have been discovered. The "Ca-rich" transient is one such newly discovered type of explosive transient (Kawabata et al. 2010; Perets et al. 2010; Kasliwal et al. 2012; Jacobson-Galán et al. 2020b; Lee et al. 2019). Their spectra commonly (if not always) show helium absorption lines around the maximum light, and most of these transients are classified into Type Ib SNe (SNe Ib) according to the classical scheme. However, they gradually start to show observational properties different from those of the classical SNe Ib after the luminosity maximum (e.g., Lunnan et al. 2017); the Ca emission lines quickly develop as early as ∼1 month after the maximum, while the oxygen forbidden lines are quite weak.

The origin of the Ca-rich transients is still a subject of active debate. They are generally discovered in a remote location from a putative host galaxy (Kasliwal et al. 2012; Lunnan et al. 2017), indicating that they originate in old populations. The old stellar population environment leads to models of white dwarf (WD) explosions (Lyman et al. 2013, 2014, 2016), exemplified by the .Ia explosion, i.e., helium detonation on a surface of a WD (Shen et al. 2010). The old environment is also consistent with a binary system involving a neutron star (NS); for example, NS–WD binaries have also been suggested as a possible origin (Lyman et al. 2014).

At the discovery of the Ca-rich transient class before this constraint from the environment had been established, one of the first suggestions regarding their origin was an explosion of a relatively low-mass He or C + O star that represents an SN from the lowest mass range to become core-collapse SNe (CCSNe; Kawabata et al. 2010). Kawabata et al. (2010) pointed out that the dominance of the Ca emissions over the oxygen emissions (i.e., deficiency in the oxygen emissions) in their spectra could be understood in the context of an explosion of such a relatively low-mass He (or C+O) progenitor (see Maeda et al. 2007; Fang et al. 2019). They also argued that the rapid evolution seen in the Ca-rich transient is a natural consequence of such a scenario; this is around a boundary between the SN explosion (either by an Fe-core collapse or ONeMg-core electron capture) and WD formation, and thus predicts small ejecta mass, i.e., $< 0.5 M_{\odot}$ (Tauris et al. 2013; Moriya et al. 2017a). The explosion energy and the ejected mass of the newly-formed ^{56}Ni are also predicted to be small (Suwa et al. 2015; Yoshida et al. 2017; Müller et al. 2018). These features are consistent with the observational properties of the Ca-rich transients, which show low expansion velocities and low luminosity.

Hereafter, we refer to the explosion of a relatively low-mass He or C + O star as the low-mass stripped-envelope SNe (SESNe). In the stellar evolution theory, one way to form such a low-mass He or C + O progenitor star is a close binary evolution with an NS companion (see also García-Berro et al. 2017; Neunteufel et al. 2019; Shen et al. 2019). In particular, if the He or C + O progenitor fills the Roche lobe, it is called the "ultra-stripped envelope SN" scenario (Tauris et al. 2013, 2015). The ultra-stripped envelope SN is a subcategory of the low-mass SESN, and they are expected to show similar observational properties. One critical difference might be the expected absence of hydrogen feature in the former, while in the latter there could be hydrogen features in the earliest spectra because a small amount of the hydrogen layer may still be left at the time of the SN explosion.

The ultra-stripped envelope SN scenario is a leading model toward the formation of double NS binaries that will merge within the Hubble time, and thus identification of ultra-stripped envelope SNe is an important topic in gravitational wave astronomy as well. Moreover, elucidating the nature of low-mass SESNe, and thus further defining the boundary between SN and non-SN, could shed light on SN progenitor evolution and the explosion mechanism.

Given the old stellar environment of the sites where Ca-rich transients are discovered, it is unlikely that the low-mass SESN is the origin of the bulk of Ca-rich transients, since it should represent a young population. However, it is still possible that a fraction of Ca-rich transients may come from low-mass SESNe, which may further contain ultra-stripped envelope SNe (Tauris et al. 2015; Moriya et al. 2017a). Among some candidates for low-mass SESNe, two Ca-rich transients are accompanied by intensive spectral series and multiband light curves. These two SNe, iPTF16hgs and iPTF14gqr, are indeed either Ca-rich transients or peculiar transients that share some properties with the Ca-rich transient class. iPTF16hgs was located at ∼6 kpc away from the core of its star-forming host galaxy, and thus its progenitor could be much younger than most Ca-rich transients. De et al. (2018a) argued that the origin of iPTF16hgs was a low-mass SESN, while the possibility of a WD eruptive event was not rejected. Further, De et al. (2018b) suggested that iPTF14gqr, which has some similarities to other Ca-rich transients (see Section 3 for details), is a robust candidate to be an ultra-stripped envelope SN. It was located in a tidally interaction spiral galaxy at ∼15 kpc away from the spiral arm (See Section 4.4).

Interestingly, both iPTF16hgs and iPTF14gqr show double-peaked light curves, where the first component rapidly declines in a few days to a week. This feature is reminiscent of the so-called "cooling-envelope emission" frequently observed for

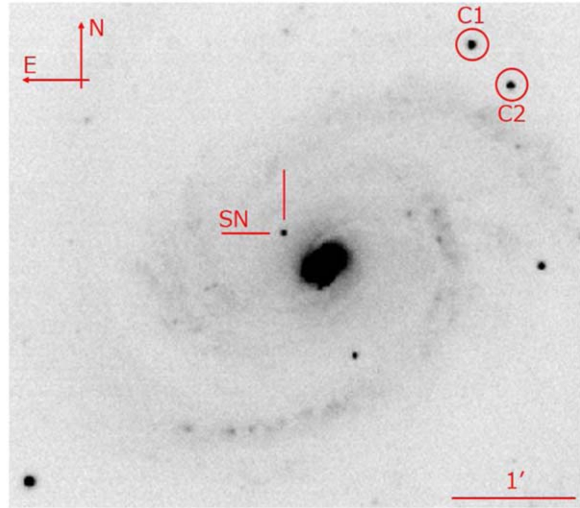

Figure 1. *R*-band image of SN 2019ehk in host galaxy M100 (NGC 4321) taken at $t = 12.2$ days using HOWPol. Open circles denote the comparison stars used for the photometric measurement. Magnitudes of these comparison stars are given by Wang et al. (2008).

CCSNe either with an extended envelope or a dense circumstellar material (CSM; Ofek et al. 2010; Chevalier & Irwin 2011; Piro 2015; Sapir & Waxman 2017). For iPTF16hgs, De et al. (2018a) interpreted this as the cooling-envelope emission of a progenitor with a radius of $\sim 10\,R_{\odot}$, which is consistent with a CCSN from a He star and its early spectra classified as an SN Ib. For iPTF14gqr, De et al. (2018b) suggested that the early emission lines are associated with a dense and "confined" CSM, as is similar to those frequently inferred for CCSNe (Gal-Yam et al. 2014; Yaron et al. 2017; Förster et al. 2018).

Given the possible link between a fraction of Ca-rich transients and the low-mass SESNe including the ultra-stripped envelope SNe, even a single new addition of a low-mass SESN candidate in the Ca-rich transient class is highly important, both in searching for candidate low-mass SESNe and ultra-stripped envelope SNe, as well as in understanding the nature (s) of Ca-rich transients. We here present such a new example, SN 2019ehk. It was discovered at α (J2000) = $12^{\rm h}22^{\rm m}56^{\rm s}.150$, δ (J2000)=$+15°49'34''.03$ by Jaroslaw Grzegorzek (Grzegorzek 2019), in the well-known spiral galaxy M100 (NGC 4321), whose distance is well-established through the Cepheid ($m - M = 30.91 \pm 0.14$; see Freedman et al. (2001)). The projected position of the explosion site is close to the core of NGC4321 (Figure 1). The explosion site is on a dust lane of a spiral arm. The apparently young environment indicates that it is originated from a massive star. Indeed, it has been classified as an SN Ib from early spectroscopic observation (Dimitriadis et al. 2019).

In this paper, we present properties of SN 2019ehk. In Section 2, we describe our observations and data reduction. In Section 3, we present its spectral and light curve properties, and we classify it as a Ca-rich transient. We further show that it has a double-peaked light curve. Comparisons of the observational properties of SN 2019ehk and those of iPTF16hgs, iPTF14gqr, and other (canonical) Ca-rich transients are also presented in Section 3. In Section 4, we discuss properties and the origin of SN 2019ehk. We suggest that this is yet another candidate for a low-mass SESN, perhaps with a wider separation from a companion NS than the ultra-stripped envelope SN; it may be a

Table 1
Log of the Optical Photometry of SN 2019ehk

MJD	Epoch (day)	*B* (mag)	*V* (mag)	*R* (mag)	*I* (mag)	Instruments
58604.7	−11.6	16.91(0.11)	16.05(0.05)	15.67(0.04)	15.20(0.03)	HOWPol
58605.5	−10.8	16.92(0.04)	16.05(0.03)	15.51(0.04)	15.04(0.03)	HOWPol
58606.6	−9.7	17.46(0.03)	16.43(0.02)	15.75(0.02)	15.26(0.02)	HOWPol
58607.6	−8.7	18.06(0.18)	16.69(0.12)	16.02(0.03)	15.54(0.04)	HOWPol
58608.6	−7.7	18.18(0.03)	16.86(0.02)	16.09(0.02)	15.58(0.02)	HOWPol
58609.6	−6.7	18.30(0.11)	16.77(0.04)	16.00(0.02)	15.46(0.02)	HOWPol
58610.6	−5.7	18.11(0.05)	16.64(0.03)	15.90(0.02)	15.35(0.02)	HOWPol
58612.6	−3.7	18.01(0.04)	16.51(0.02)	15.76(0.02)	15.13(0.02)	HOWPol
58614.6	−1.7	18.09(0.07)	16.46(0.03)	15.63(0.02)	14.99(0.02)	HOWPol
58615.7	−0.6	18.11(0.05)	16.45(0.02)	15.61(0.02)	14.93(0.02)	HOWPol
58619.5	3.2	⋯	16.79(0.05)	15.74(0.03)	14.99(0.03)	HOWPol
58624.5	8.2	⋯	17.27(0.03)	16.12(0.03)	15.28(0.02)	HOWPol
58626.6	10.3	⋯	17.50(0.03)	16.31(0.02)	15.40(0.02)	HOWPol
58628.5	12.2	⋯	17.65(0.03)	16.48(0.02)	15.49(0.02)	HOWPol
58629.6	13.3	⋯	17.83(0.19)	16.64(0.14)	15.52(0.05)	HOWPol
58632.5	16.2	⋯	17.85(0.04)	16.69(0.03)	15.64(0.02)	HOWPol
58634.5	18.2	⋯	17.97(0.06)	16.83(0.03)	15.68(0.02)	HOWPol
58637.6	21.3	⋯	18.15(0.15)	16.96(0.04)	15.68(0.03)	HOWPol
58639.5	23.2	⋯	18.21(0.05)	17.01(0.04)	15.76(0.03)	HOWPol
58646.5	30.2	⋯	18.71(0.1)	17.30(0.04)	15.84(0.03)	HOWPol

Note. Only Galactic extinction has been corrected for.

precursor of a double NS binary, which is unlikely to merge within a Hubble time. We further argue that a fraction of Ca-rich transients belong to this class. The paper is closed in Section 5 with conclusions. Throughout this paper, t denotes the rest-frame phase since the *R*-band second maximum (MJD 58616.3, corresponding to $t = 0$). The explosion date is estimated as MJD 58601.9 ($t = -14.4$ days), defined as the date between the last nondetection (MJD 58601.3) and the earliest detection (MJD 58602.5; Joel Shepherd).

2. Observations and Data Reduction

The optical imaging data were obtained using the Hiroshima One-shot Wide-field Polarimeter (HOWPol; Kawabata et al. 2008) and the Hiroshima Optical and Near-InfraRed Camera (HONIR; Akitaya et al. 2014). These instruments are installed on the 1.5-m Kanata telescope at the Higashi-Hiroshima Observatory, Hiroshima University. We obtained *BVRI*-band images using HOWPol over 14 nights from 2019 May 1.7 ($t = -11.6$ days) to 12.3 July 2019 ($t = 30.2$ days). For the photometric measurements, we adopted the Point-Spread Function (PSF) photometry using the DAOPHOT task (Stetson 1987) in IRAF (Tody 1986, 1993). For the calibration of optical photometry, we used the magnitudes of the nearby comparison stars given by Wang et al. (2008). The derived optical magnitudes are summarized in Table 1. Figure 2 shows the multiband light curves. Only the Galactic extinction has been corrected for in this figure (see Section 3.2). We also plot data from other sources, represented by the open circles (clear-band magnitudes reported by Joel Shepherd and by Jaroslaw Grzegorzek; a cyan-ATLAS-band magnitude by ATLAS).[16]

Non-filter optical imaging data in the field around the discovery date were taken with a new wide-field CMOS sensor camera Tomo-e Gozen (Sako et al. 2018) on the 1.05 m KisoSchmidt telescope during a wide-field high-cadence transient survey. We picked up the survey data on two epochs during the same night of 2019 April 27. For each epoch, the data consist of 12 contiguous 0.5 s exposures. SN 2019ehk is not detected, and we derived 5σ upper limits on the subtracted images, using the deep co-added Tomo-e Gozen image taken in 2020 as a reference image. The derived upper limits (relative to Pan-STARRS *r*-band) are 16.42 and 17.97 mag on MJD 58600.4 and 58600.5 days, respectively.

All the magnitudes are given in the Vega system throughout this paper, unless mentioned otherwise. The double peaks are seen in the optical light curves, and the second peak is reached in the *R* band at 14.4 days after the estimated explosion date; it is defined as $t = 0$ days in this paper.

The JHK_s-band imaging data were obtained using HONIR on seven nights between 2019 May 5.4 ($t = -9.7$ days) and 2019 May 24.5 ($t = 11.2$ days). We took the images using a dithering mode to accurately subtract a bright foreground sky.

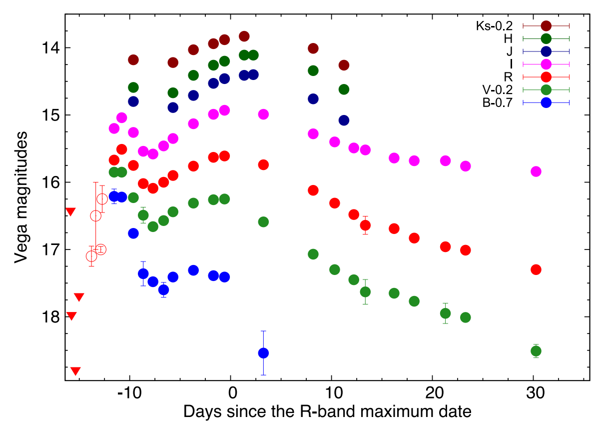

Figure 2. Optical and NIR light curves of SN 2019ehk. Estimated explosion date is $t = -14.4$ days (see Section 1). Only the Galactic extinction (Schlafly & Finkbeiner 2011) has been corrected for. Host extinction has not been corrected for in this figure (see Section 3.2).

[16] https://wis-tns.weizmann.ac.il/object/2019ehk

Table 2
Log of the NIR Photometry of SN 2019ehk

MJD	Epoch (day)	J (mag)	H (mag)	K_s (mag)	Instruments
58606.6	−9.7	14.80(0.02)	14.59(0.02)	14.38(0.03)	HONIR
58610.6	−5.7	14.89(0.02)	14.67(0.02)	14.42(0.03)	HONIR
58612.6	−3.7	14.71(0.03)	14.41(0.02)	14.23(0.05)	HONIR
58614.6	−1.7	14.53(0.02)	14.26(0.02)	14.14(0.03)	HONIR
58615.7	−0.6	14.46(0.02)	14.2(0.02)	14.08(0.03)	HONIR
58617.6	1.3	14.41(0.02)	14.11(0.02)	14.03(0.02)	HONIR
58618.5	2.2	14.40(0.02)	14.11(0.02)	…	HONIR
58624.5	8.2	14.76(0.02)	14.34(0.02)	14.21(0.02)	HONIR
58627.5	11.2	15.08(0.02)	14.62(0.02)	14.46(0.03)	HONIR

Table 3
Log of the Spectroscopic Observations of SN 2019ehk

MJD	Epoch (day)	Exposure (sec)	Coverage	Resolution	Instruments
58608.6	−7.7	3600	4500–9000 Å	400	HOWPol
58610.6	−5.7	2700	4500–9000 Å	400	HOWPol
58612.5	−3.8	3600	4000–8900 Å	500	KOOLS-IFU
58614.6	−1.7	2700	4500–9000 Å	400	HOWPol
58615.6	−0.7	2700	4500–9000 Å	400	HOWPol
58624.5	8.2	3600	4500–9000 Å	400	HOWPol
58632.6	16.3	3600	4500–9000 Å	400	HOWPol
58670.3	53.9	1800	5200–9800 Å	400	GMOS
58825.6	280.3	1200	5000–9000 Å	500	FOCAS

We reduced the data and performed photometry following the standard procedure for NIR data based on the PSF photometry method in IRAF. The magnitudes were calibrated using the magnitudes of nearby comparison stars given in the 2MASS catalog (Persson et al. 1998). The derived JHK_s-band magnitudes and their light curves are given in Table 2 and Figure 2, respectively.

The spectra are shown in Figure 3, and the log of our spectroscopic observations is shown in Table 3. We performed optical spectroscopic observations using HOWPol on six nights between 2019 May 5.5 ($t = -4.7$ days) and 2019 May 29.5 ($t = 30.5$ days). We used a grism with a spectral resolution of $R \sim 400$ and a spectral coverage of 4500–9000 Å. We observed spectroscopic standard stars on the same nights for the flux calibration. For the wavelength calibration, we used sky emission lines taken in the object frames. The strong atmospheric absorption bands around 6900 Å and 7600 Å have been removed using the spectra of hot standard stars.

We also obtained an optical spectrum using the Kyoto Okayama Optical Low-dispersion Spectrograph with an integral field unit (KOOLS-IFU; Matsubayashi et al. 2019) attached to the 3.8-m Seimei telescope of Kyoto University on 2019 May 9 ($t = -3.8$ days). We used the VPH-blue grism with a wavelength resolution of $R \sim 500$ and a wavelength coverage of 4000–8900 Å. To remove cosmic ray events, we used the L. A. Cosmic pipeline (van Dokkum 2001). The data reduction was performed using the Hydra package in IRAF (Barden et al. 1994; Barden 1995) and a reduction software specifically developed for KOOLS-IFU data. The flux was calibrated using the data of a spectroscopic standard star taken

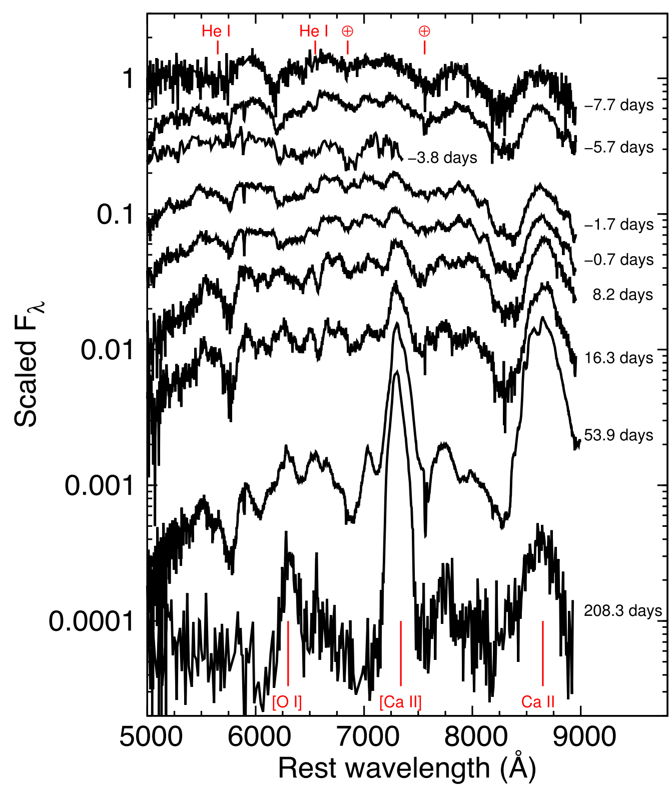

Figure 3. Spectral evolution of SN 2019ehk. Epoch of each spectrum is given with respect to the R-band maximum (see Section 1). Only the Galactic extinction has been corrected for.

on the same night. For the wavelength calibration, we used arc lamp (Hg and Ne) data.

Another optical spectrum was obtained using the Gemini Multi-Object Spectrograph (GMOS; Allington-Smith et al. 2002; Hook et al. 2004) attached to the Gemini telescope on 2019 July 6.3 ($t \sim 54$ days). We used the *R*400 grism with a slit width of 1 arcsec. The flux calibration was performed using a spectrum of a spectrophotometric standard star taken in the same night. The data reduction was carried out using Gemini IRAF.[17]

In addition, we obtained an optical spectrum using the Faint Object Camera and Spectrograph (FOCAS; Kashikawa et al. 2002) attached to the Subaru Telescope on 2019 December 8.6 ($t \sim 208$ days). We used the 300*B* grism with a slit width of 0.8 arcsec. The flux calibration and the data reduction were performed in the same way as those with HOWPol, except that the arc lamp (Th-Ar) data and skylines were used for the wavelength calibration.

3. Results

3.1. Spectra

Figure 3 shows the spectral evolution of SN 2019ehk from the end of the first peak ($t = -7.7$ days) to the tail phase ($t = 208.3$ days). Several absorption lines are identified in the spectra before the second maximum ($t < 0$ days): He I λ5876, He I λ 6678, Si II λ 6355, O I λ 7774, and the Ca II NIR triplet. Overall features indicate that SN 2019ehk is a member of SNe Ib, according to the standard criteria. The strong Na I D narrow absorption line at the redshift of the host galaxy M100 ($z \sim 0.002$) indicates that the absorption within the host galaxy is substantial (see Section 3.2 for further details). After the second peak ($t > 0$ days), spectral features quickly evolve. Prominent Ca II and [Ca II] emission lines are developed already at $t = 16.3$ days, showing a rapid transition to the nebular phase. These features, a rapid evolution to the nebular phase and the prominent Ca emissions, are characteristics of a Ca-rich transient.

In Figure 4, we compare SN 2019ehk with SN Ib 2008D (Modjaz et al. 2009), SN IIb 1993J (Barbon et al. 1995), iPTF14gqr (De et al. 2018b), iPTF16hgs (De et al. 2018a), and Ca-rich transient PTF10iuv (Kasliwal et al. 2012) at $t \sim 0$ days (i.e., around the maximum brightness). Overall, the spectrum of SN 2019ehk is similar to those of SN Ib 2008D and the Ca-rich transients (iPTF16hgs and PTF10iuv). Indeed, there are no significant differences between the Ca-rich transients and (some of the) SNe Ib at this stage. At a closer look, the line profiles of He I, O I, and Fe II seen in SN 2019ehk show a better match to those of the Ca-rich transients than SN 2008D. The spectrum of iPTF14gqr in this early phase is distinct from the Ca-rich transients, confirming the argument by De et al. (2018b) that it should not be classified as a "canonical" Ca-rich transient.

Emission lines of Ca II and [Ca II] become prominent for iPTF16hgs and PTF10iuv at $t \sim 20$ days (Figure 5), which is the definition of the "Ca-rich" transient class (Kawabata et al. 2010; Perets et al. 2010). SN 2019ehk shows a strikingly similar spectrum. While the absorption lines of He I are still visible, the spectra of the Ca-rich transients are distinct from SNe Ib at this phase, and thus SN 2019ehk should be definitely

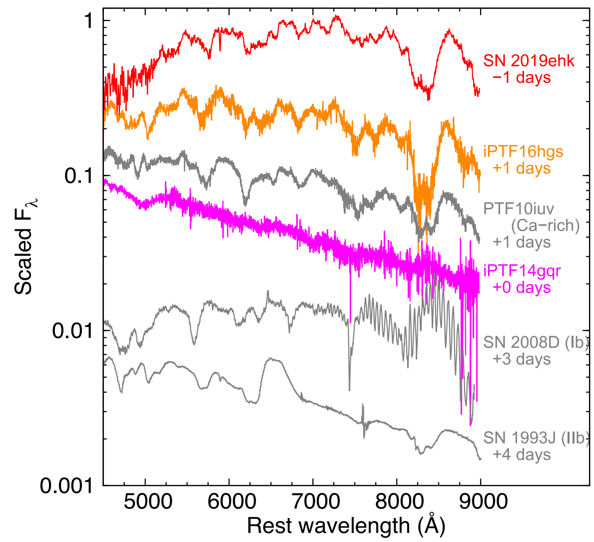

Figure 4. Spectrum of SN 2019ehk around the second peak ($t \sim 0$ days), compared with the following objects: SN Ib 2008D (Modjaz et al. 2009), SN IIb 1993J (Barbon et al. 1995), iPTF16hgs (De et al. 2018a), iPTF14gqr (De et al. 2018b), and (canonical) Ca-rich transient PTF10iuv (Kasliwal et al. 2012), at similar epochs. Only the Galactic extinction has been corrected for in SN 2019ehk.

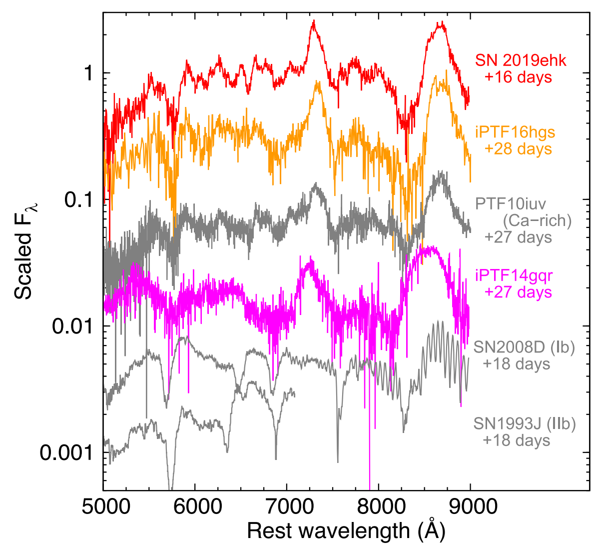

Figure 5. Same as Figure 4, but at $t \sim 20$ days.

classified as a Ca-rich transient, not as a canonical SN Ib. Interestingly, iPTF14gqr comes to resemble the other Ca-rich transients at this phase, showing strong [Ca II] and Ca II NIR triplet. Therefore, iPTF14gqr can also be classified as a Ca-rich transient according to the standard criterion. However, we should note that iPTF14gqr shows broader Ca emissions than the others, and some lines identified in the other Ca-rich transients are not visible in its spectrum. As such, iPTF14gqr could be classified as a peculiar Ca-rich transient, which might indicate that its origin is different from the canonical Ca-rich transients.

The difference between (normal) SNe Ib and Ca-rich transients becomes more obvious in the later phases. All the Ca-rich transients show strong [Ca II] and Ca II emission lines, and weak or no [O I] at $t \sim 55$ days (Figure 6). The velocity

[17] https://www.gemini.edu/node/11823

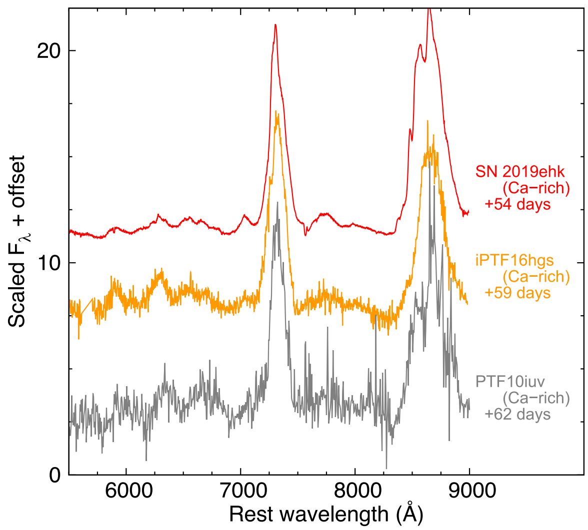

Figure 6. Spectrum of SN 2019ehk at a late phase ($t = 54$ days) as compared with those of Ca-rich transients iPTF16hgs (De et al. 2018a) and PTF10iuv (Kasliwal et al. 2012) at similar epochs. Only the Galactic extinction has been corrected for in SN 2019ehk.

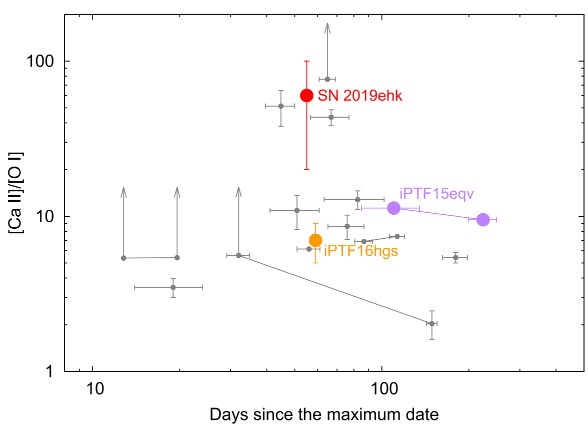

Figure 7. Ratio of [Ca II] /[O I] compared with those for other Ca-rich transients, including iPTF16hgs (Milisavljevic et al. 2017; De et al. 2018a; Prentice et al. 2020).

seen in SN 2019ehk, as measured from the full width at half maximum of a Gaussian function fitted to the [Ca II] profile, is $\sim$5300 km s^{-1} . This is again similar to other (canonical) Ca-rich transients (Kasliwal et al. 2012) (e.g., as compared to PTF10iuv). The [O I] seen in SN 2019ehk is very weak even among Ca-rich transients.

Figure 7 shows the evolution of the [Ca II] /[O I] ratio as compared with those measured from spectra of a sample of Ca-rich transients presented by Valenti et al. (2014). The [Ca II] / [O I] ratio of SN 2019ehk at $t \sim 54$ days is measured to be 60 ± 40, which is within the range generally seen in the Ca-rich transients, and is among the largest.

Figure 8 shows the evolution of the He I line velocities of SN 2019ehk. The velocities are derived from a Gaussian fit to the He I λ5876 and He I λ6678 absorption line profiles. We do not see a clear evolution in the velocity of He I λ 5876, but it is likely contaminated by Na I D. The velocity measured for He I λ 6678 is around 6500 km s^{-1} at $t \sim -5$ days, and declines to $\sim$3000 km s^{-1} at $t \sim 54$ days. The velocity and its evolution here roughly overlap with those of iPTF16hgs.

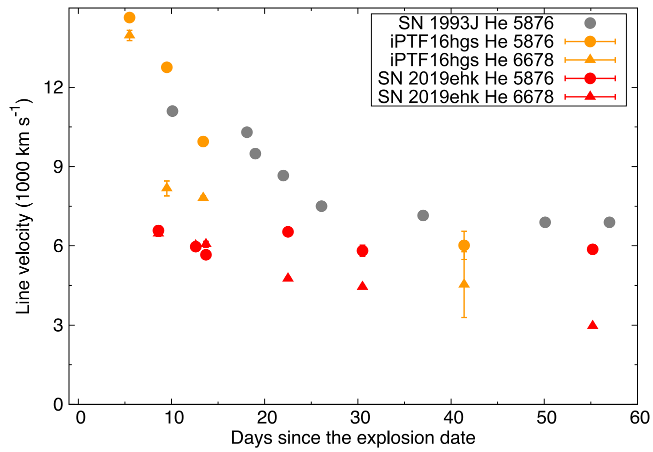

Figure 8. He I λ5876 and λ6678 velocity evolution of SN 2019ehk as compared with those of SN IIb 1993J (Barbon et al. 1995) and iPTF16hgs (De et al. 2018a). Explosion date is estimated as $t = -14.4$ days.

The spectral features and their evolution show that SN 2019ehk clearly belongs to the Ca-rich transient class. It shows spectral properties very similar to those of iPTF16hgs, and these two objects also share striking similarities in their light curves (see Section 3.3). iPTF14gqr is distinct from SN 2019ehk, iPTF16hgs, and other Ca-rich transients in terms of spectral evolution, while its similarities with regard to late phase spectrum and light-curve properties (Section 3.3) to SN 2019ehk and iPTF16hgs suggest a link among these three objects.

3.2. *Extinction Correction*

The Galactic extinction is negligibly small for SN 2019ehk ($E(B-V) = 0.026$ mag; see Schlafly & Finkbeiner (2011)). However, the extinction within the host galaxy along the line of sight toward SN 2019ehk is highly uncertain. Our spectra show a very deep Na I D absorption line, indicating substantial extinction within the host galaxy (see Figure 3). We measure the equivalent width (EW) as 3.2 ± 0.3 Å; this is beyond the applicability of the extinction–EW relation suggested by Poznanski et al. (2010).

Given the similarities between SN 2019ehk and iPTF16hgs, we could match the spectra of these two objects in order to constrain the extinction. Figure 9 shows the spectral comparison at $t \sim 0$ days, with different values of $E(B-V)$ applied to SN 2019ehk ($E(B-V) = 0.5$ and 1.0 mag). With $E(B-V) = 0.5$ mag, the two spectra match quite well. The blackbody temperature of SN 2019ehk is $\sim$5400 K and $\sim$8100 K, assuming respective extinctions of $E(B-V) = 0.5$ and 1.0 mag. Since the spectral features of SN 2019ehk are similar to those of iPTF16hgs, the temperature should not be very different between the two objects; as a rough estimate, if the temperature were different by $\gtrsim 50\%$, the differences in the spectral features would likely become significant (Nugent et al. 1995). This places a rough upper limit of $E(B-V) \sim 1.0$ mag for SN 2019ehk.

To compare the color evolution of SN 2019ehk and other Ca-rich transients, we convert the magnitudes of SN 2019ehk to the SDSS system using the relations given by Jordi et al. (2006). In the comparison using the SDSS system, we apply the AB magnitude. We also confirm that these SDSS (AB) magnitudes are consistent with those estimated from the spectra of SN 2019ehk. Figure 10 shows the $g-r$ color

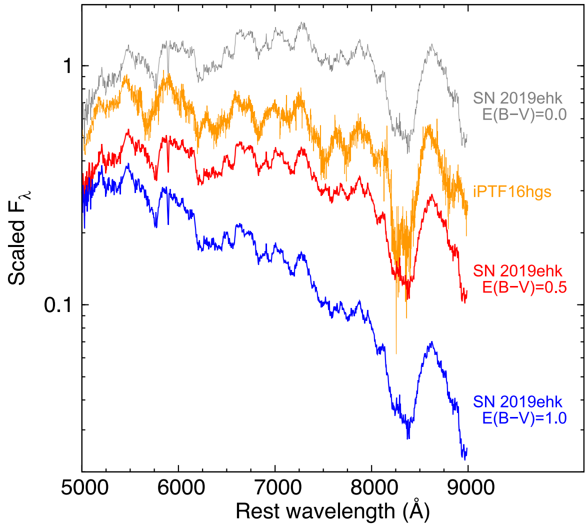

Figure 9. Extinction-corrected spectra of SN 2019ehk as compared to iPTF16hgs, with different values assumed for the host extinction: $E(B-V)=0.5$ (red) and 1.0 (blue). Gray line shows the original spectrum of SN 2019ehk at $t=-1$ days. Green line shows the spectrum of iPTF16hgs at $t=1$ days.

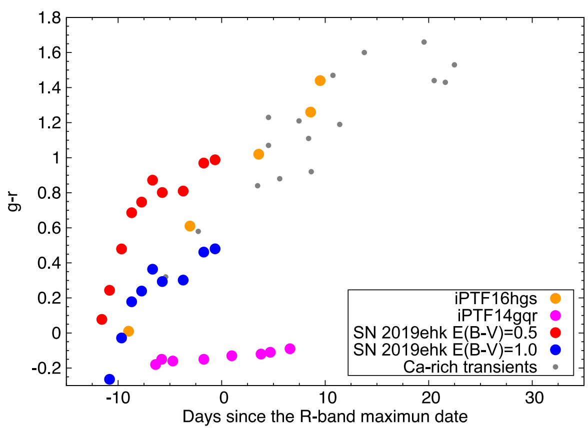

Figure 10. The $g-r$ color evolution of SN 2019ehk as compared with iPTF14gqr, iPTF16hgs, and other Ca-rich transients (PTF10iuv, PTF11kmb, PTF12bho). Red and blue filled circles denote the color of SN 2019ehk, corrected for the host extinction, and assuming $E(B-V)=0.5$ and $E(B-V)=1.0$ mag, respectively. SDSS magnitudes are given in the AB system.

evolution of SN 2019ehk as compared to iPTF16hgs, iPTF14gqr, and other Ca-rich transients. The color evolution of SN 2019ehk roughly matches those of iPTF16hgs and other Ca-rich transients, for $E(B-V)$ between 0.5 and 1.0 mag. This range is consistent with that from the spectral matching to iPTF16hgs. Therefore, we estimate the host extinction to be between $E(B-V)=0.5$ and 1.0 mag.

One issue we face when trying to obtain the absolute magnitudes is determining the value of R_V. Usually, the Galactic value ($R_V=3.1$) is adopted for CCSNe, while it is suggested to be lower ($R_V\sim 2$) for SNe Ia (Wang et al. 2008). The host extinction is usually negligible for Ca-rich transients, and thus the typical value for Ca-rich transients is uncertain. In this paper, we adopt the Galactic value, i.e., $R_V=3.1$, which is more likely the case than the smaller value, given our interpretation of SN 2019ehk, independent from R_V, as a member of CCSNe (see Section 4). While adopting $R_V\sim 2$ will

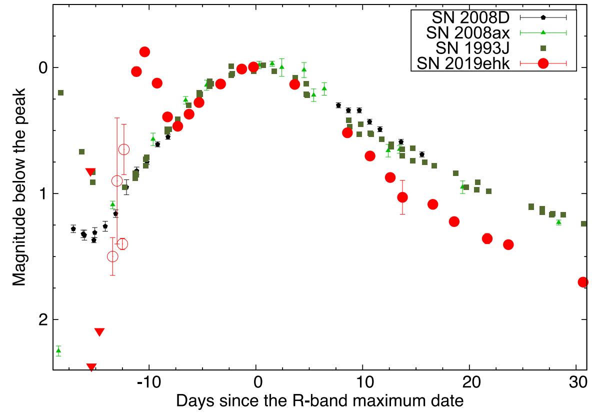

Figure 11. *R*-band light curve of SN 2019ehk compared to those of well-observed SNe: SN Ib 2008D (Modjaz et al. 2009), SN IIb 2008ax (Pastorello et al. 2008), and SN IIb 1993J (Richmond et al. 1996). All the magnitudes are relative to the peak.

reduce the estimated absolute magnitude by ∼0.5–1.0 mag, this would not affect our main conclusions, given that we already consider a range of $E(B-V)=0.5$–1.0 mag.

3.3. Light Curves

Figure 2 shows our multiband light curves. Note that these magnitudes are corrected only for the Galactic extinction (see Section 3.2). The light curve shows a clear rise to the first peak in the optical bands after its discovery. Similar initial emissions were also detected for iPTF14gqr and iPTF16hgs, while the rising part toward the first peak was missed for both of them. This early emission has not been seen in the other Ca-rich transients. The first peak is reached at $t=-10.8$ days for SN 2019ehk.

The decline rate after the second peak (between $t=-0.6$ and $t=13.3$ days) is 0.09, 0.07, and 0.05 mag day^{-1} in the *V*, *R*, and *I* bands, respectively. After $t\sim 13.3$ days, the decline becomes slower. The decline rate between $t=26$ and 38 days is 0.05, 0.05, and 0.03 mag day^{-1}in the *V*, *R*, and *I* bands, respectively. A bluer band shows a steeper decline.

We compare the *R*-band light curve of SN 2019ehk to those of canonical SNe IIb and Ib in Figure 11. The same comparison, but for the *r* band (see Section 3.2), is shown with iPTF14gqr, iPTF16hgs, and other Ca-rich transients in the top panel of Figure 12. In these figures, we also plot the magnitudes of SN 2019ehk reported by other sources (see Section 2). These early points are shown here only for demonstration purpose, because of the differences in the band passes even though the central wavelengths are close to the *R* or *r* band. For the sake of comparison, we shift the light curves vertically to match to the peak magnitude of SN 2019ehk, and horizontally to match to the peak date.

The middle and bottom panels of Figure 12 show the absolute magnitude light curves of SN 2019ehk in the *r* and *g* bands, respectively, as compared with those of iPTF14gqr, iPTF16hgs, and other (canonical) Ca-rich transients (see Section 3.2). To show the uncertainty associated with the extinction, the absolute magnitudes of SN 2019ehk are corrected for host excitation with $E(B-V)=0.5$ mag (red filled circles) or $E(B-V)=1.0$ mag (blue).

Figure 11 shows that the light-curve evolution is much faster for SN 2019ehk than for the well-studied SNe IIb and Ib. It is especially clear in terms of the rising time to the second peak

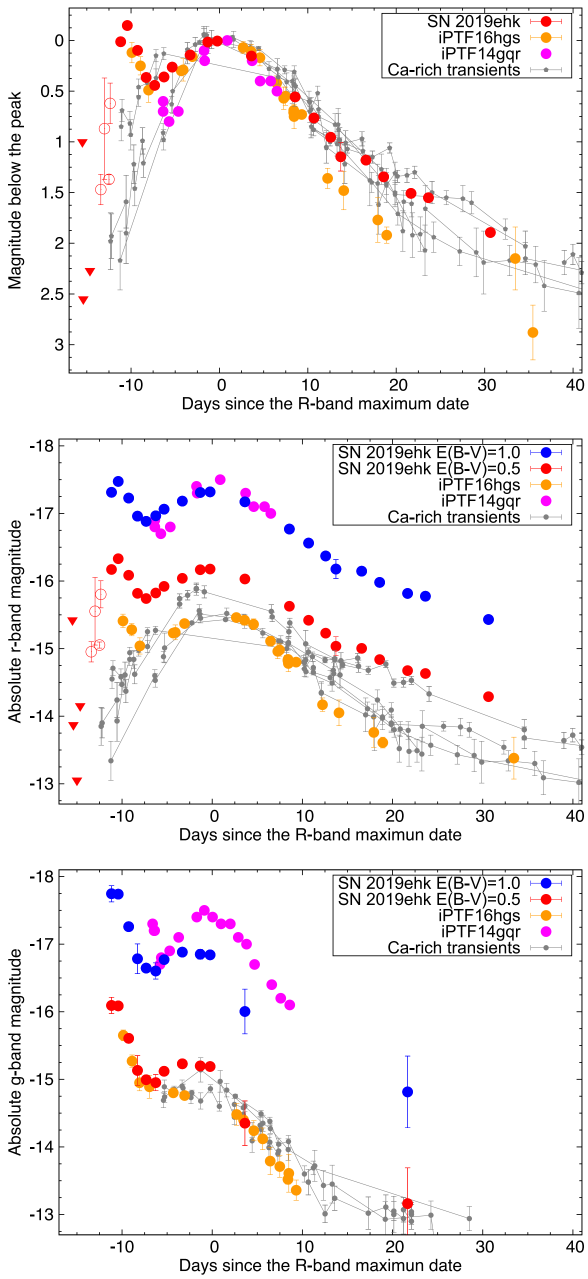

Figure 12. Top panel shows the r-band light curve of SN 2019ehk compared with iPTF14gqr (De et al. 2018b), iPTF16hgs (De et al. 2018a), and other Ca-rich transients PTF10iuv, PTF11kmb, and PTF12bho (Kasliwal et al. 2012; Lunnan et al. 2017). Middle and bottom panels are the same as the top, but with magnitudes shown in the absolute magnitude scale, in the r band (middle) and the g band (bottom), given in the AB system. Light curve of SN 2019ehk is shown for two different values of the host extinction: $E(B-V)=0.5$ mag (red filled circle) and $E(B-V)=1.0$ mag (blue one). Magnitudes of SN 2019ehk are given in AB magnitude. In these figures, $R_V = 3.1$ is assumed.

since the (estimated) explosion date: 22.7, 20.0, 23.6, and 12.7 days for SNe 1993J, 2008D, 2008ax, and 2019ehk, respectively. The same tendency is also seen in the decline rate after the second maximum: 0.045, 0.05, 0.055, and 0.07 mag day^{-1} in SNe 1993J, 2008D, 2008ax, and 2019ehk, respectively.

SN 2019ehk, iPTF16hgs, and other Ca-rich transients show similar rising times, as seen in Figure 12. For example, the rising time and the decline rate for iPTF16hgs in the r band are 12.7 days and 0.10 mag day^{-1}, respectively, which are both similar to those of SN 2019ehk. iPTF14gqr shows a faster rise and fall than these objects, suggesting a smaller amount of ejecta. In any case, the light-curve evolution of iPTF14gqr is qualitatively similar to SN 2019ehk and the Ca-rich transients, being much faster than canonical SNe Ib.

The decline rate of SN 2019ehk after $t \sim 10$ days is within a range observed for the Ca-rich transients, although it is on the slower side. On the other hand, iPTF16hgs shows the fastest decline among the Ca-rich transients. If SN 2019ehk and iPTF16hgs belong to the same subpopulation within the Ca-rich transient class (along with iPTF14gqr, as argued in this paper), it might suggest that this subpopulation has much more diverse properties than the other (main) population within the Ca-rich transient class.

The r-band peak magnitude of SN 2019ehk at $t \sim 0$ days is $\sim$1 mag brighter than those of PTF10iuv and iPTF16hgs in the case of $E(B-V) = 0.5$ mag.[18] Even taking the uncertainty in the host extinction into account, SN 2019ehk is much more luminous in its (second) peak than the bulk of the Ca-rich transients. It can be compared to the peak luminosity of iPTF14gqr, which also shows a distinctly brighter peak than the other comparison objects.

The first peak is reminiscent of early emission from some CCSNe, exemplified by SN IIb 1993J. The magnitude of this emission relative to the second-peak magnitude, as well as the declining rate (and the duration from the estimated explosion date), are indeed similar between SN 1993J and SN 2019ehk. The emission is well-understood as the “cooling envelope emission” for the case of SN 1993J, with its extended H-rich progenitor (Richmond et al. 1996). Similar early emission is also seen for iPTF14gqr and iPTF16hgs, while such a feature has not been detected for the other (canonical) Ca-rich transients. The existence of the first peak would suggest that SN 2019ehk, iPTF14gqr, and iPTF16hgs may form a subpopulation within the Ca-rich transient class (or a population of explosions that resemble the canonical Ca-rich transients, in terms of observational features). The similarities in the properties of the first peak may further suggest that they are related to the deaths of massive stars (Section 4.2 for further details).

4. Discussion

Based on the observational data presented in Section 3, we discuss properties and a possible origin of SN 2019ehk. We also discuss a possible relation of SN 2019ehk to iPTF14gqr, iPTF16hgs, and the Ca-rich transients in general. In Section 4.1, we estimate the properties of the ejecta from the observational properties around the second peak. The origin of the first peak is discussed in Section 4.2. In Section 4.3, we argue that SN 2019ehk is an explosion of a massive star, specifically a low-mass SESN. It would not, however, be a system experiencing a substantial Roche lobe mass transfer toward the SN explosion, suggesting that this may be a variant of the ultra-stripped envelope SN but with a wider binary separation.

[18] Only if we were to adopt a combination of $E(B-V)$ ~0.5 mag and $R_V \sim 2$ mag for the host extinction (i.e., the assumptions leading to the minimal amount of the extinction) would the absolute magnitude of SN 2019ehk be similar to that of iPTF16hgs.

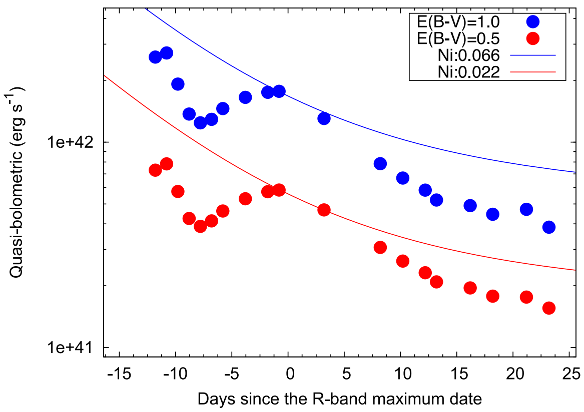

Figure 13. Bolometric light curves(s) of SN 2019ehk as compared to the ^{56}Ni/Co/Fe decay full-trapping model light curve(s) (Nadyozhin 1994), with different assumptions on the host extinction, $E(B-V)=0.5$ (red circles and line) and $E(B-V)=1.0$ mag (blue), and $R_V=3.1$. Explosion date is estimated as $t=-14.4$ days.

4.1. Properties of the Ejecta and Implications for the Progenitor

First, we construct a quasi-bolometric light curve of SN 2019ehk by integrating the spectral energy distribution (SED) in the B, V, R, and I bands. The integration is performed by interpolating the SED with trapezium functions. The conversion from the observed magnitude into the flux is carried out using the filter function (Bessell 1990) and the zero-point flux in each band.

We show the bolometric light curve in Figure 13. The bolometric light curve is constructed assuming two different values of the host extinction: $E(B-V)=0.5$ and 1.0 mag (see Section 3.2). The ratio of the optical flux (in the B, V, R, and I bands) to the total flux is assumed to be that seen in typical SNe Ib/c (60%; Drout et al. 2014), given the similarity in the maximum spectra; we note that this is largely consistent with the value adopted for iPTF16hgs (De et al. 2018a). The first peak of SN 2019ehk is also confirmed in the quasi-bolometric light curve. The second-peak luminosity, $L_{\rm peak}$, is $\sim 6\times10^{41}$ erg s^{-1} in the case of low extinction ($E(B-V)=0.5$ mag), which already exceeds the typical range found for the canonical Ca-rich transients (Kasliwal et al. 2012; Lunnan et al. 2017). It could even be as bright as $L_{\rm peak}\sim 2\times10^{42}$ erg s^{-1} if $E(B-V)=1.0$ mag, making it comparable to the peak luminosity of iPTF14gqr. The rise time to the second peak is estimated to be 14.4 days, which is similar to iPTF16hgs (12.6 days; De et al. 2018a) and other Ca-rich transients.

We calculate the ^{56}Ni mass, M(^{56}Ni), as $0.02-0.07$ $M_\odot$ from the second-peak luminosity (Arnett 1982), where the range reflects the extinction uncertainties. Even with $E(B-V)=0.5$ mag, this is larger than the values found for most of the Ca-rich transients (Kasliwal et al. 2012) including iPTF16hgs (De et al. 2018a). The estimated ^{56}Ni mass is between iPTF16hgs and iPTF14gqr, or similar to iPTF14gqr, depending on the treatment of the host extinction toward SN 2019ehk.[19]

We estimate the kinetic energy and the ejecta mass for SN 2019ehk from the analysis of the light-curve evolution. We fit the r-band light curve of SN 2019ehk to that of iPTF16hgs by stretching the light-curve width around the second maximum. We then obtain the ratio of the timescale of SN 2019ehk to iPTF16hgs as $\sim$1.2.

Figure 8 suggests that the expansion velocities are similar between SN 2019ehk and iPTF16hgs, with a ratio of $\sim$0.8 between two objects. We further test this via the overall spectral property. After bending the second-maximum ($t\sim0$ days) spectrum of SN 2019ehk to match to the continuum of iPTF16hgs (Figure 9), we introduce an artificial shift in the wavelength to the spectrum of SN 2019ehk, to find the best match in the positions of the absorption minima of different lines. We thereby find that the ratio of the line velocities of SN 2019ehk to iPTF16hgs is on average $v_{\rm 19ehk}/v_{\rm 16hgs}\sim0.8$, i.e., consistent with the estimate using the He velocity.

We then convert these ratios in the light-curve widths and the expansion velocities to the ejecta mass ($M_{\rm ej}$) and the kinetic energy of the ejecta ($E_{\rm k}$), using the following relations:

$$\tau \propto M_{\rm ej}^{3/4}\cdot E_{\rm k}^{-1/4}, \tag{1}$$

$$v_{\rm ej} \propto M_{\rm ej}^{-1/2}\cdot E_{\rm k}^{1/2}. \tag{2}$$

For the normalization in this scaling method, we use the ejecta properties estimated for iPTF16hgs ($M_{\rm ej}=0.38\,M_\odot$ and $E_{\rm k}=2.3\times10^{50}$ erg; see De et al. (2018a)). We then obtain $M_{\rm ej}=0.43$ $M_\odot$ and $E_{\rm k}=1.7\times10^{50}$ erg for SN 2019ehk.

These properties are similar to those obtained for iPTF16hgs (and the other Ca-rich transients in general), as expected from the similar properties seen in their light curves and spectra. The ejecta mass is smaller than that of iPTF14gqr, while the kinetic energy is similar ($M_{\rm ej}=0.2\,M_\odot$ and $E_{\rm k}=2\times10^{50}$ erg; see De et al. (2018b)). These properties are consistent with the slower evolution and lower line velocities in SN 2019ehk versus those in iPTF14gqr.

4.2. Analysis of the First Peak

Here, we investigate the origin of the first peak in the light curves. Given the large uncertainty in the host extinction, we consider a range of the possible extinction between $E(B-V)=0.5$ and 1.0 mag as roughly constrained by the color at the second peak (see Section 3.2). The possible energy source of the first peak is roughly divided into two categories: the radioactivity and the shock interaction. In Section 4.3, we argue against the former scenario, and thus in this section we focus on the shock-interaction power. This is further divided into two classes of the mechanism: the shock-cooling emission and the ongoing shock-powered emission. We discuss these scenarios one by one in this section.

The first peak observed for SN 2019ehk is reminiscent of the so-called cooling-envelope emission frequently observed for CCSNe with an extended envelope (e.g., see SN IIb 1993J in Figure 11), where the thermal energy deposited by the propagation of the shock wave is diffused out in the cooling timescale. The mechanism is indeed not limited to a "stellar envelope," but rather is applicable to a "confined" CSM as long as the CSM is already swept up by the ejecta and behaves like a cooling envelope.

For the analysis of this process, we follow the formalism presented by Piro (2015). In doing this, we use a semi-analytic code developed by Maeda et al. (2018) to simulate a similar emission process. We calibrated the code by comparing the output to the results of Piro (2015) for the same parameter set. Indeed, De et al. (2018a) used the same formalism to analyze

[19] The M(^{56}Ni) of SN 2019ehk can be similar to that of iPTF16hgs only for the (unlikely) combination of $E(B-V)\sim0.5$ mag and $R_v\sim2$ for the host extinction.

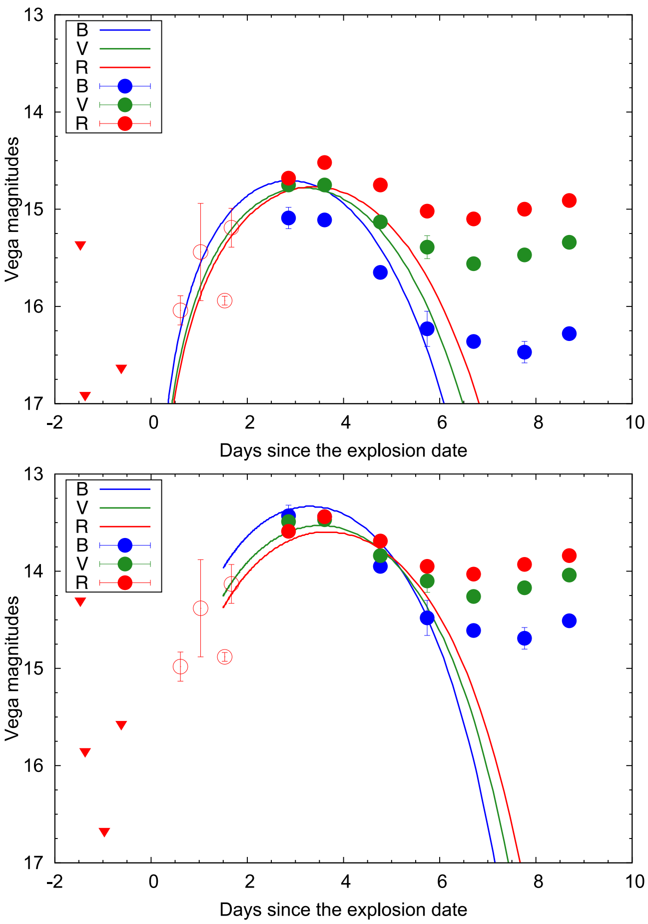

Figure 14. The B-, V-, and R-band light curves of SN 2019ehk and the cooling-envelope/CSM models that fit to the V-band light curve. Host extinction is assumed to be $E(B-V)=0.5$ (top) or $E(B-V)=1.0$ mag (bottom). Explosion date is estimated as $t=-14.4$ days.

the first peak seen in iPTF16hgs. We have also confirmed that we obtain a result consistent with that of De et al. (2018a), if we use the same input parameters; this guarantees a fair comparison between the natures of SN 2019ehk and iPTF16hgs.

As the input parameters, we adopt $M_{\rm ej}=0.43\ M_\odot$ for the ejecta mass and $E_{\rm k}=1.7\times10^{50}$ erg for the kinetic energy (see Section 4.1). The luminosity is sensitive to the radius of the envelope (or CSM) while the diffusion timescale is so to the envelope (CSM) mass, and there is no degeneracy between these two parameters to derive. We first try to obtain a rough match to the V-band light curve, and the same model is adopted to generate the B- and R-band light curves.

As shown in Figure 14, we can obtain a reasonable fit to the early V-band light curve. The envelope/CSM mass is $\sim$0.04–0.05 $M_\odot$ irrespective of the extinction assumption. The outer radius of the envelope/CSM is sensitive to the assumed extinction: 130 $R_\odot$, 300 $R_\odot$, and 1500 $R_\odot$ for $E(B-V)=0.5$, 0.7, and 1.0 mag, respectively. While the mass is similar to that derived for iPTF16hgs (De et al. 2018a), the radius required for SN 2019ehk is substantially larger. This is a result of the brighter first peak luminosity ($L_{\rm bump}$) in SN 2019ehk even for $E(B-V)=0.5$ mag.

We note that the expected model color is far too blue to be consistent with the observations of SN 2019ehk, as long as $E(B-V)<1.0$ mag. The cooling-envelope emission predicts that the V-band peak is realized when the photospheric temperature decreases to $\sim$10,000–20,000 K, as an outcome of the shift of the blackbody peak from the UV to the optical bands. However, the observed color of the first peak is red ($V-R>0$ mag) if $E(B-V)<1.0$ mag. There is then no solution to explain the color via the cooling-envelope emission under the low-extinction assumption (Figure 14).

A physically reasonable solution with the cooling-envelope emission model can be found only if we assume a high value of the extinction ($E(B-V)=1.0$ mag; see Figure 14). The derived radius can be as large as $\sim$1500 $R_\odot$. This is comparable even to one of the largest SN IIP progenitors discovered through the pre-explosion image analysis (Huang et al. 2018). Our spectra do not exhibit any hydrogen absorption features, and such a large and He-rich "envelope" is physically not realized. On the other hand, the mass and radius here are very similar to those suggested for the "confined" CSM around CCSNe commonly inferred through the flash spectroscopy (Gal-Yam et al. 2014; Yaron et al. 2017) or early light-curve behaviors (Moriya et al. 2017b, 2018; Morozova et al. 2017, 2018; Förster et al. 2018). We suggest that this can be interpreted as the existence of the confined CSM around SN 2019ehk, which might further support its origin as a core collapse of a massive star. The corresponding mass-loss rate is $\sim$1.5 $M_\odot$ yr^{-1}, assuming a mass-loss velocity of 1000 km s^{-1}. This is high due to the large wind velocity assumed here, but it involves a large uncertainty—even more than an order of magnitude.

As clarified above, another emission mechanism is required if $E(B-V)<1.0$ mag. An alternative mechanism is the situation in which the ejecta is still propagating within the optically thick CSM at the first peak of the light curve. This allows a larger photospheric radius as well as a lower temperature, and thus a redder color. If $E(B-V)=0.5$ mag, the blackbody fit to the SED at the first peak suggests a photospheric temperature of $\sim$7000 K. The observed luminosity and temperature for the case of $E(B-V)=0.5$ mag indicate a blackbody radius of $\sim$11,000 $R_\odot$ (i.e., $\sim8\times10^{14}$ cm). Similarly, if we assume $E(B-V)=0.7$ mag, then the photospheric temperature and the radius are $\sim$8500 K and $\sim$9400 $R_\odot$ ($\sim7\times10^{14}$ cm), respectively. This is again within the range suggested for the confined CSM. We can derive the CSM density (and thus the mass-loss rate) under this ongoing shock interaction model, through the peak luminosity (interaction power) and the peak duration (diffusion timescale) (Moriya & Maeda 2014).[20] The mass-loss rate thus derived is $\sim4\times10^{-3}$ $M_\odot$ yr^{-1}, assuming a constant wind velocity of $\sim$1000 km s^{-1}, which is the velocity seen in iPTF14gqr (De et al. 2018b); this velocity is also expected for a He star progenitor. Again, the required CSM density (the mass-loss rate) and the size are within the range estimated for the confined CSM around CCSNe.

The narrow emission lines of hydrogen in the earliest spectrum of SN 2019ehk were reported by Dimitriadis et al. (2019) and discussed in Jacobson-Galán et al. (2020a). This indicates that the ongoing interaction model may be more likely, while the shock-cooling scenario is not immediately

[20] The required CSM mass is much smaller than the cooling-envelope/CSM case, as the ongoing shock is much more efficient in the energy conversion without substantial adiabatic cooling (e.g., Maeda et al. 2018). Note also that the uncertainty in the luminosity within a factor of two would not alter the mass-loss rate estimate (Moriya & Maeda 2014).

Table 4
Physical Parameters of SN 2019ehk

E(B-V) (mag)	$R_{\rm peak}$ (mag)	$L_{\rm peak}$ ($\times 10^{42}$ erg s^{-1})	$L_{\rm bump}$ ($\times 10^{42}$ erg s^{-1})	M(^{56}Ni) ($M_\odot$)	CSM Radius ($R_\odot$)	Mass-loss Rate ($M_\odot$ yr^{-1})
0.5	−16.29	0.583	0.783	0.022	11,000	4×10^{-3}
0.7	−16.71	0.897	1.27	0.037	9400	4×10^{-3}
1.0	−17.35	1.77	2.72	0.066	1500	1.5

Note. Here, $M_{\rm ej}$=0.43 $M_\odot$ and $E_{\rm k}$=1.7×10^{50} erg, irrespective of the extinction. The wind velocity ($v_{\rm w}$) is assumed to be 1000 km s^{-1} in order to estimate the mass-loss rate; for a different value of the assumed wind velocity, the mass-loss rate is scaled as $\dot{M} \propto (v_{\rm w}/1000)$ km s^{-1}. In these estimates, $R_V = 3.1$ is assumed.

rejected. The progenitor system of SN 2019ehk including these early emission lines in the spectrum is discussed in Section 4.3.

In summary, we suggest two possible interpretations: the cooling envelope/CSM emission (for $E(B-V) \sim 1.0$ mag) or the ongoing CSM interaction (for $E(B-V) < 1.0$ mag) (see Section 4.3 for details regarding the difficulties presented by another mechanism where it is powered by radioactivity, e.g., by ^{56}Ni). The results of this analysis are summarized in Table 4, together with the properties derived from the second peak, where $R_{\rm peak}$ is the R-band peak magnitude of SN 2019ehk at $t \sim 0$ days. While the two scenarios involve different mechanisms and result in different natures of the CSM, we come to the same conclusions in qualitative terms. In both cases, there is a dense CSM around SN 2019ehk. The progenitor might experience (unknown) unstable activity in the final stage of the stellar evolution of the massive star (Fuller & Ro 2018).

4.3. The Low-mass SESN as a Progenitor System

The ejecta properties of SN 2019ehk, iPTF14gqr, and iPTF16hgs are generally consistent with the expectations for a low-mass ($<2M_\odot$) He (or C+O) star explosion corresponding to a main-sequence mass of 8–12 $M_\odot$, which defines a boundary between a CCSN explosion and a WD formation (Kawabata et al. 2010). In terms of the binary evolution, such a low-mass He or C + O star progenitor is a system of interest in the formation of double NS binaries; if a companion star is an NS, the low-mass SESN can leave a bound double NS binary, while the explosion of a more massive star should disrupt the progenitor binary system. The low-mass SESNe include the ultra-stripped envelope SN with an NS comparison (Tauris et al. 2013, 2015), which has been actively debated as a promising pathway to form double NS binaries. Indeed, De et al. (2018b) suggested iPTF14gqr as a robust candidate to be an ultra-stripped envelope SN. The scenario favored for iPTF16hgs (De et al. 2018a) is also the ultra-stripped envelope SN, while an eruptive event related to a WD is not rejected. In this paper, we suggest that SN 2019ehk is yet another candidate for a low-mass SESN. We note that a similar scenario has also been proposed by De et al. (2021).

It is possible that SN 2019ehk might have left a double NS binary. However, the orbital separation of the post explosion binary is likely wider than the genuine ultra-stripped envelope SNe. This is thus a candidate system for double NSs with a large separation, which will not merge within the Hubble time (Tauris et al. 2017), and such systems are seen in Galactic double NSs systems (Farrow et al. 2019). SN 2019ehk is thus an interesting object that could potentially provide insight regarding the conditions and fraction leading to the ultra-stripped envelope SNe among the low-mass SESN systems, which may then be linked to the formation scenario of double NSs.

The diversities seen in these objects are in line with the expectation from a core-collapse event of a massive star, as there can be diversities in the progenitor stars, e.g., in the progenitor mass and in the properties of the envelope at the time of the explosion (Tauris et al. 2015). Indeed, given the low-mass ejecta, a small difference in the progenitor mass in the low-mass SESN scenario can easily lead to a large diversity in the observational properties (Moriya et al. 2017a; Suwa et al. 2015; Yoshida et al. 2017; Müller et al. 2018). For example, Tauris et al. (2015) predict that the ejecta mass ranges from $\sim$0.01 $M_\odot$ to $\sim$0.5 $M_\odot$ for the progenitors leading to ultra-stripped envelope SNe. The range covers the properties derived for SN 2019ehk, iPTF14gqr, and iPTF16hgs.

SN 2019ehk, iPTF14gqr, and iPTF16hgs share a unique observational property; they show a "first" peak with a duration of a few days observed in the optical wavelength. This feature can be naturally interpreted as the existence of a substantial amount of CSM, as has been interpreted for many CCSNe. The models based on an old system, e.g., a WD, have difficulties creating such a short-duration early emission. The so-called .Ia scenario would create a double-peaked light curve in the "bolometric" luminosity due to existence of powering radioactive species at different layers. However, in this model, the first peak is generally in the UV and the second peak is in the optical; the optical light curve is indeed predicted not to show the double peaks (Shen et al. 2010). An exception is the double-detonation model of a sub-Chandrasekhar mass WD, which could create the double peaks in the optical (Jiang et al. 2017; Maeda et al. 2018). However, given the relatively low luminosity of SN 2019ehk and the other objects (as compared to SNe Ia), this will result in substantial absorption by various Fe-peak lines at the second peak (Maeda et al. 2018), and the resulting spectrum would never resemble that of an SN Ib.

Through "flash spectroscopy," De et al. (2018b) suggested the existence of a confined CSM around iPTF14gqr. For iPTF16hgs, the properties of the first peak are explained by the cooling-envelope emission from a He-rich envelope, without the need for a dense CSM. The first peak observed for SN 2019ehk can be explained either by a very dense and confined CSM (if the extinction is high) or a moderately dense CSM (if the extinction is low; see Section 4.2). Either way, irrespective of an association with a He-rich envelope or a confined CSM, the double-peak light curve suggests a link to the CCSN, especially to the low-mass SESN. Given the classification of SN 2019ehk and iPTF16hgs as Ca-rich transients, as well as the similarities of iPTF14gqr to these objects, the existence of multiple populations is indicated within the Ca-rich transients (see Section 4.4).

Indeed, the difference in the properties of the first peak may indicate further subclassification among the low-mass SESNe. As mentioned in Section 4.2, the narrow emission lines of hydrogen in the earliest spectrum of SN 2019ehk were reported by Dimitriadis et al. (2019) and discussed in Jacobson-Galán et al. (2020a). Importantly, this indicates that the He star progenitor did not experience a strong Roche lobe mass transfer toward the SN explosion for the case of SN 2019ehk. On the other hand, iPTF14gqr showed noticeable He lines but not hydrogen lines in its flash spectrum. This variation may be expected in a low-mass SESN with a NS companion star; in such a scenario, the low-mass He star is first produced via common envelope interaction with an NS companion (Tauris et al. 2013). If the reduction in the orbital separation in the common envelope phase is substantial, the progenitor star will further fill the Roche lobe, and the entire H envelope (and perhaps further, the He layer as well) may be stripped away to become an ultra-stripped envelope SN. On the other hand, if the binary separation after the common envelope phase is modest, a small amount of H envelope will be left, and this could be the situation for SN 2019ehk.

4.4. A Subpopulation within Ca-rich Transients?

Most Ca-rich transients show a large offset from a host galaxy (Lunnan et al. 2017). This indicates old stellar populations (e.g., an explosion or an eruptive event of a WD) as their origin. Kasliwal et al. (2012) and Lunnan et al. (2017) showed that the (canonical) Ca-rich transients have homogeneous luminosity distribution, indicating similar ^{56}Ni masses. The evolutions in the spectra and light curve also show homogeneous natures (Section 3; see also De et al. (2018a)).

However, there are some Ca-rich transients, including SN 2019ehk, that show star-forming activity in their explosion sites. SN 2019ehk is on a dust lane along a spiral arm of M100. Another Ca-rich transient, iPTF16hgs, is located at ∼6 kpc away from the core of a star-forming galaxy (De et al. 2018a), which is atypical as a site of the Ca-rich transient. As yet another example, a peculiar Ca-rich transient, iPTF15eqv, is located on an arm of a spiral galaxy. Early phase data for iPTF15eqv are missing, as it was discovered after the maximum, but it is definitely much brighter than the canonical Ca-rich transients with an estimated ^{56}Ni mass of M(^{56}Ni) = 0.07 $M_\odot$ for iPTF15eqv (Milisavljevic et al. 2017). Among the low-mass SESN candidates discussed in this paper, iPTF14gqr does not clearly show star-forming activity in its explosion site; it is offset by ∼30 kpc from the core of a star-forming galaxy (or ∼15 kpc from the nearest spiral arm), which is consistent with the old environment generally derived for the Ca-rich transients, while the host galaxy shows a tidally interacting environment (De et al. 2018b).

SN 2019ehk, iPTF16hgs, and iPTF14gqr share a distinct feature in their light curves; a first peak with a duration of a few days to a week.[21] This is not seen in the other canonical Ca-rich transients. Analysis of the first peaks suggests that they originate in the CCSN events. At the same time, they also show some diversities in their observational properties. iPTF16hgs is nearly indistinguishable from the canonical Ca-rich transients, except for the first peak and its potentially young environment. iPTF14gqr shows characteristics quite different from those of the Ca-rich transients, e.g., its early-phase spectra and the double-peaked light curve, while it evolves to resemble the canonical Ca-rich transients in a late phase. The almost featureless spectra of iPTF14gqr around the peak are likely due to the high luminosity and temperature as well as the high expansion velocities. The properties of SN 2019ehk are in between those of iPTF16hgs and iPTF14gqr; spectroscopically, it is indistinguishable from the canonical Ca-rich transients, but it shows a high luminosity, a clear first peak, and a star-forming environment.

As a consequence of the diversity in the observational properties, the inferred properties of the ejecta and circumstellar environment are also diverse. The ejected ^{56}Ni masses span from M(^{56}Ni) = 0.01 $M_\odot$ for iPTF16hgs to M(^{56}Ni) = 0.05 $M_\odot$ for iPTF14gqr. SN 2019ehk is in between. The ejecta mass may range from ∼0.2$M_\odot$ (iPTF14gqr; see De et al. (2018b)) to ∼0.4 $M_\odot$ (iPTF16hgs and SN 2019ehk; see De et al. (2018a) and this paper). There also seems to be some diversity in the nature of the circumstellar environment (Section 4.2).

In summary, we suggest that SN2019ehk, iPTF16hgs, and iPTF14gqr (and potentially iPTF15eqv) form a subpopulation within the Ca-rich transient class. They not only explode within the young environment (with the possible exception of iPTF14gqr) but also have observational properties beyond the diversity seen in the canonical Ca-rich transients. Their properties are summarized in Table 5, together with those of PTF10iuv as a representative of the canonical Ca-rich transients. We identify four such objects (SN 2019ehk, iPTF14gqr, iPTF15eqv, and iPTF16hgs), i.e., ∼10% of the whole sample of Ca-rich transients. Note that the fraction here might be an overestimate, given the systematically higher peak immensities for these events versus those of the canonical Ca-rich transients. The rate of Ca-rich transient is estimated as ∼33–95% of SNe Ia in the local universe, which corresponds to ∼10–30% of CCSNe. Therefore, the rate of this subpopulation (including SN 2019ehk) is roughly ∼1%–3% of CCSNe, or even larger. This rate is marginally consistent with the expectation for the ultra-stripped envelope SN scenario to be a main evolutionary pathway toward double NS binaries (Tauris et al. 2013, 2015), i.e., 0.1%–1%. Indeed, while the estimate here is very rough, the relatively high rate of the subpopulation under consideration might indicate that it would contain not only the extreme case of a ultra-stripped envelope SNe (i.e., a close binary with a NS), but those of a low-mass helium star explosion in a binary system with a massive main-sequence star, or in a binary with an NS but with a large binary separation, which may indeed be the case for SN 2019ehk (Section 4.3).

5. Summary

We have performed optical and near-infrared observations of SN 2019ehk. While it was initially reported as an SN Ib, it shows a rapid development of [Ca II] and Ca II emission lines. The overall spectral evolution matches well to that of the Ca-rich transients. It is thus definitely classified as a Ca-rich transient. Note that normal SNe Ib and Ca-rich transients can be indistinguishable in the early-phase spectra, and thus this change in classification is not surprising.

Despite the spectral similarity, SN 2019ehk shows clear differences in its light-curve properties versus those of the canonical Ca-rich transients. The peak magnitude can be up to 2 mag brighter than the typical value seen in the Ca-rich

[21] SN 2019dge also shows the same feature (Yao et al. 2020).

Table 5
Properties of Ca-rich Transients

Objects	$M(^{56}\mathrm{Ni})$ ($M_\odot$)	Double Peak	Environments	References
SN 2019ehk	0.02–0.07	YES	Young	This paper
iPTF16hgs	0.008	YES	Young	De et al. (2018a)
iPTF15eqv	0.05–0.07	⋯	Young	Milisavljevic et al. (2017)
iPTF14gqr	0.05	YES	Old/Young?	De et al. (2018b)
PTF10iuv[a]	0.016	NO	Old	Kasliwal et al. (2012)

Note.
[a] See Section 3.1.

transients, depending on the uncertain host extinction. Furthermore, SN 2019ehk shows a clear first peak, which is not observed for the canonical Ca-rich transients.

From the properties of the second peak, assuming it is powered by the ^{56}Ni/Co/Fe decay chain, we derived the ejecta mass and the explosion energy as $M_{\mathrm{ej}} = 0.43$ $M_\odot$ and $E_{\mathrm{k}} = 1.7 \times 10^{50}$ erg, respectively. The mass of ^{56}Ni has a large uncertainty due to the host extinction, but is constrained to be 0.02–0.07 $M_\odot$. We interpret the origin of the first peak as the emission associated with a dense and potentially confined CSM whose properties are within the range of those inferred for CCSNe. These properties suggest that SN 2019ehk is a variant of CCSNe. Indeed, these properties are largely consistent with the expectations from an explosion of a low-mass He star ($\sim$2 $M_\odot$). Low-mass SESNe are related to, and indeed include, ultra-stripped envelope SNe in terms of their observational SN properties and evolutionary pathway.

We identify at least three (peculiar) Ca-rich transients (SN 2019ehk, iPTF16hgs, and iPTF14gqr) that show peculiar properties beyond the diversity within the canonical Ca-rich transients. As a distinguishing feature, they all show a double-peaked light curve, indicating a CCSN origin. Interestingly, two of them (SN 2019ehk and iPTF16hgs) have the explosion-site environment atypical as a Ca-rich transient, indicating that their progenitor stars belong to a young population. The environment of iPTF14gqr is within the diversity seen for the Ca-rich transients, but its association with the young environment is not rejected (De et al. 2018b). While the pre-maximum data are missing, a peculiar Ca-rich transient iPTF15eqv also shares some properties with these peculiar Ca-rich transients.

We suggest that these Ca-rich transients form a (young) subpopulation within the Ca-rich transient class. Their properties can be explained as resulting from an explosion of a low-mass ($\sim$2$M_\odot$) He star, i.e., the low-mass SESN scenario, and this scenario explains why the observational properties within this subpopulation are much more diverse than those seen in the canonical Ca-rich transients. These candidates may well include systems with an NS companion star, which can be further divided into two categories: NS binaries with a close orbital separation (i.e., ultra-stripped envelope SNe) and those with a wide separation. There could also be systems with a massive star companion, like the bulk of SESNe.

Our finding of the low-mass SESNe as a subpopulation of Ca-rich transients suggests an interesting direction in the search for ultra-stripped envelope SN candidates to aid in understanding the evolutionary pathway toward double NS binaries: high-cadence searches for transients to catch the first distinct peak, and continuous follow-up observations to observe the development of the Ca-rich transients' signatures in the late phase.

The authors acknowledge Raffaella Margutti, Dan Milisavljevic, and Wynn Jacobson-Galan for stimulating discussion, after their manuscript and this manuscript on SN 2019ehk were both posted on arXiv. The GMOS observation, S19A-051, was conducted via the time exchange program between Gemini and the Subaru Telescope. The FOCAS observation, S19B-055, was conducted at the Subaru Telescope, and the authors thank Kentaro Aoki and the Subaru telescope staff for the observation. This research has made use of the NASA/IPAC Extragalactic Database (NED), which is operated by the Jet Propulsion Laboratory, California Institute of Technology, under contract with the National Aeronautics and Space Administration. This research has made use of the NASA/IPAC Infrared Science Archive, which is operated by the Jet Propulsion Laboratory, California Institute of Technology, under contract with the National Aeronautics and Space Administration. Keiichi Maeda acknowledges support provided by the Japan Society for the Promotion of Science (JSPS) through KAKENHI Grants JP17H02864, JP18H04585, JP18H05223, JP20H00174, and JP20H04737. Masayuki Yamanaka is supported by the Grants-in-Aid for Young Scientists of the Japan Society for the Promotion of Science (JP17K14253). Koji S. Kawabata acknowledges support provided by the Japan Society for the Promotion of Science (JSPS) through KAKENHI Grant JP18H03720. Umut Burgaz acknowledges support provided by the Turkish Scientific and Technical Research Council (TÜBİTAK−2211C and 2214A) Tomoki Morokuma acknowledges support provided by the Japan Society for the Promotion of Science (JSPS) through KAKENHI Grants JP16H02158 and JP18H05223.

ORCID iDs

Keiichi Maeda https://orcid.org/0000-0003-2611-7269
Masayuki Yamanaka https://orcid.org/0000-0001-9456-3709
Masaomi Tanaka https://orcid.org/0000-0001-8253-6850
Miho Kawabata https://orcid.org/0000-0002-4540-4928
Takashi J. Moriya https://orcid.org/0000-0003-1169-1954
Koji S. Kawabata https://orcid.org/0000-0001-6099-9539
Nozomu Tominaga https://orcid.org/0000-0001-8537-3153
Tomoki Morokuma https://orcid.org/0000-0001-7449-4814
Ryou Ohsawa https://orcid.org/0000-0001-5797-6010
Takashi Nagao https://orcid.org/0000-0002-3933-7861
Ji-an Jiang https://orcid.org/0000-0002-9092-0593
Makoto Uemura https://orcid.org/0000-0002-7375-7405
Hiroshi Akitaya https://orcid.org/0000-0001-6156-238X
Mahito Sasada https://orcid.org/0000-0001-5946-9960
Hiroyuki Maehara https://orcid.org/0000-0003-0332-0811

References

Akitaya, H., Moritani, Y., Ui, T., et al. 2014, Proc. SPIE, 9147, 91474O
Allington-Smith, J., Murray, G., Content, R., et al. 2002, PASP, 114, 892
Arnett, W. D. 1982, ApJ, 253, 785
Barbon, R., Benetti, S., Cappellaro, E., et al. 1995, A&AS, 110, 513
Barden, S. C. 1995, Proc. SPIE, 2476, 2
Barden, S. C., Armandroff, T., Muller, G., et al. 1994, Proc. SPIE, 2198, 87
Bessell, M. S. 1990, PASP, 102, 1181
Chevalier, R. A., & Irwin, C. M. 2011, ApJL, 729, L6

De, K., Fremling, U. C., Gal-Yam, A., Kasliwal, M. M., & Kulkarni, S. R. 2021, ApJL, 907, L18
De, K., Kasliwal, M. M., Cantwell, T., et al. 2018a, ApJ, 866, 72
De, K., Kasliwal, M. M., Ofek, E. O., et al. 2018b, Sci, 362, 201
Dimitriadis, G., Siebert, M. R., Kilpatrick, C. D., et al. 2019, Transient Name Server Classification Report, 2019-675, IAU Supernova Working Group
Drout, M. R., Chornock, R., Soderberg, A. M., et al. 2014, ApJ, 794, 23
Fang, Q., Maeda, K., Kuncarayakti, H., Sun, F., & Gal-Yam, A. 2019, NatAs, 3, 434
Farrow, N., Zhu, X.-J., & Thrane, E. 2019, ApJ, 876, 18
Förster, F., Moriya, T. J., Maureira, J. C., et al. 2018, NatAs, 2, 808
Freedman, W. L., Madore, B. F., Gibson, B. K., et al. 2001, ApJ, 553, 47
Fuller, J., & Ro, S. 2018, MNRAS, 476, 1853
Gal-Yam, A., Arcavi, I., Ofek, E. O., et al. 2014, Natur, 509, 471
García-Berro, E., Badenes, C., Aznar-Siguán, G., & Lorén-Aguilar, P. 2017, MNRAS, 468, 4815
Grzegorzek, J. 2019, Transient Name Server Discovery Report, 2019-666, IAU Supernova Working Group
Hook, I. M., Jørgensen, I., Allington-Smith, J. R., et al. 2004, PASP, 116, 425
Huang, F., Wang, X.-F., Hosseinzadeh, G., et al. 2018, MNRAS, 475, 3959
Jacobson-Galán, W. V., Margutti, R., Kilpatrick, C. D., et al. 2020a, ApJ, 898, 166
Jacobson-Galán, W. V., Polin, A., Foley, R. J., et al. 2020b, ApJ, 896, 165
Jiang, J.-A., Doi, M., Maeda, K., et al. 2017, Natur, 550, 80
Jordi, K., Grebel, E. K., & Ammon, K. 2006, A&A, 460, 339
Kashikawa, N., Aoki, K., Asai, R., et al. 2002, PASJ, 54, 819
Kasliwal, M. M., Kulkarni, S. R., Gal-Yam, A., et al. 2012, ApJ, 755, 161
Kawabata, K. S., Maeda, K., Nomoto, K., et al. 2010, Natur, 465, 326
Kawabata, K. S., Nagae, O., Chiyonobu, S., et al. 2008, Proc. SPIE, 7014, 70144L
Lee, M. G., Jang, I. S., & Kang, J. 2019, ApJ, 871, 33
Lunnan, R., Kasliwal, M. M., Cao, Y., et al. 2017, ApJ, 836, 60
Lyman, J. D., James, P. A., Perets, H. B., et al. 2013, MNRAS, 434, 527
Lyman, J. D., Levan, A. J., Church, R. P., Davies, M. B., & Tanvir, N. R. 2014, MNRAS, 444, 2157
Lyman, J. D., Levan, A. J., James, P. A., et al. 2016, MNRAS, 458, 1768
Maeda, K., Jiang, J.-a., Shigeyama, T., & Doi, M. 2018, ApJ, 861, 78
Maeda, K., Kawabata, K., Tanaka, M., et al. 2007, ApJL, 658, L5
Matsubayashi, K., Ohta, K., Iwamuro, F., et al. 2019, PASJ, 71, 102
Milisavljevic, D., Patnaude, D. J., Raymond, J. C., et al. 2017, ApJ, 846, 50
Modjaz, M., Li, W., Butler, N., et al. 2009, ApJ, 702, 226
Moriya, T. J., Förster, F., Yoon, S.-C., Gräfener, G., & Blinnikov, S. I. 2018, MNRAS, 476, 2840
Moriya, T. J., & Maeda, K. 2014, ApJL, 790, L16
Moriya, T. J., Mazzali, P. A., Tominaga, N., et al. 2017a, MNRAS, 466, 2085
Moriya, T. J., Yoon, S.-C., Gräfener, G., & Blinnikov, S. I. 2017b, MNRAS, 469, L108
Morozova, V., Piro, A. L., & Valenti, S. 2017, ApJ, 838, 28
Morozova, V., Piro, A. L., & Valenti, S. 2018, ApJ, 858, 15
Müller, B., Gay, D. W., Heger, A., Tauris, T. M., & Sim, S. A. 2018, MNRAS, 479, 3675
Nadyozhin, D. K. 1994, ApJS, 92, 527
Neunteufel, P., Yoon, S. C., & Langer, N. 2019, A&A, 627, A14
Nugent, P., Phillips, M., Baron, E., Branch, D., & Hauschildt, P. 1995, ApJL, 455, L147
Ofek, E. O., Rabinak, I., Neill, J. D., et al. 2010, ApJ, 724, 1396
Pastorello, A., Kasliwal, M. M., Crockett, R. M., et al. 2008, MNRAS, 389, 955
Perets, H. B., Gal-Yam, A., Mazzali, P. A., et al. 2010, Natur, 465, 322
Persson, S. E., Murphy, D. C., Krzeminski, W., Roth, M., & Rieke, M. J. 1998, AJ, 116, 2475
Piro, A. L. 2015, ApJL, 808, L51
Poznanski, D., Chornock, R., Nugent, P. E., et al. 2010, Sci, 327, 58
Prentice, S. J., Maguire, K., Flörs, A., et al. 2020, A&A, 635, A186
Richmond, M. W., Treffers, R. R., Filippenko, A. V., & Paik, Y. 1996, AJ, 112, 732
Sako, S., Ohsawa, R., Takahashi, H., et al. 2018, Proc. SPIE, 10702, 107020J
Sapir, N., & Waxman, E. 2017, ApJ, 838, 130
Schlafly, E. F., & Finkbeiner, D. P. 2011, ApJ, 737, 103
Shen, K. J., Kasen, D., Weinberg, N. N., Bildsten, L., & Scannapieco, E. 2010, ApJ, 715, 767
Shen, K. J., Quataert, E., & Pakmor, R. 2019, ApJ, 887, 180
Stetson, P. B. 1987, PASP, 99, 191
Suwa, Y., Yoshida, T., Shibata, M., Umeda, H., & Takahashi, K. 2015, MNRAS, 454, 3073
Tauris, T. M., Kramer, M., Freire, P. C. C., et al. 2017, ApJ, 846, 170
Tauris, T. M., Langer, N., Moriya, T. J., et al. 2013, ApJL, 778, L23
Tauris, T. M., Langer, N., & Podsiadlowski, P. 2015, MNRAS, 451, 2123
Tody, D. 1986, Proc. SPIE, 627, 733
Tody, D. 1993, in ASP Conf. Ser. 52, Astronomical Data Analysis Software and Systems II, ed. R. J. Hanisch, R. J. V. Brissenden, & J. Barnes (San Francisco, CA: ASP), 173
Valenti, S., Yuan, F., Taubenberger, S., et al. 2014, MNRAS, 437, 1519
van Dokkum, P. G. 2001, PASP, 113, 1420
Wang, X., Li, W., Filippenko, A. V., et al. 2008, ApJ, 675, 626
Yao, Y., De, K., Kasliwal, M. M., et al. 2020, ApJ, 900, 46
Yaron, O., Perley, D. A., Gal-Yam, A., et al. 2017, NatPh, 13, 510
Yoshida, T., Suwa, Y., Umeda, H., Shibata, M., & Takahashi, K. 2017, MNRAS, 471, 4275